Article

J. Biol. Regul. Homeost. Agents. 2024; 38(5): 3991–4004
https://doi.org/10.23812/j.biol.regul.homeost.agents.20243805.316

Integrated Analysis of Single-Cell RNA Sequencing and Microarray Transcriptomics Reveals Promotion of Pulmonary Arterial Hypertension Progression by POSTN-Positive Smooth Muscle Cells

Qian Gu[1,†], Yan Zhou[2,†], Lei Zhou[1,*]

[1]Department of Cardiology, The First Affiliated Hospital of Nanjing Medical University, 210029 Nanjing, Jiangsu, China
[2]Department of Pancreatic Surgery, Nanjing Drum Tower Hospital, The Affiliated Hospital of Nanjing University Medical School, 210008 Nanjing, Jiangsu, China
*Correspondence: zhoulei@njmu.edu.cn (Lei Zhou)
[†]These authors contributed equally.
Published: 1 May 2024

Background: Pulmonary arterial hypertension (PAH) is characterized by a progressive increase in pulmonary vascular resistance, culminating in right ventricular failure and heightened mortality. Utilizing bioinformatics can aid in unraveling the underlying mechanisms of various diseases. Our study aimed to elucidate the novel pathogenic role of periostin (POSTN) in PAH through bioinformatics method.

Methods: Gene expression microarray datasets and single-cell RNA sequencing (scRNA-seq) data were retrieved from the Gene Expression Omnibus. Differential expression analysis and identification of key hub genes were performed to identify crucial pathogenic genes in PAH. Functional enrichment and Gene Set Enrichment Analysis were employed to elucidate the pertinent biological functions of these key genes. A comprehensive array of bioinformatics techniques, including locus analysis, transcription factor regulation analysis, and cell interaction analysis, were further utilized to conduct an in-depth analysis of the scRNA-seq dataset. The analyses aimed to explore the association between POSTN, smooth muscle cells, and macrophages, unveiling the clinical correlation and potential pathogenic mechanisms of POSTN and PAH. Additionally, this association was validated in animal models.

Results: POSTN expression was significantly elevated in PAH ($p < 0.0001$), and was closely associated with fibroblast infiltration ($p < 0.0001$). In the scRNA-seq dataset, POSTN expression was observed in fibroblasts and smooth muscle cells (SMCs), with POSTN as the most differentially expressed gene between the SMCs of PAH and donors. POSTN-positive ($POSTN^+$) SMCs were notably enriched in the microenvironment of PAH. Activation of hypoxia-inducible factor 1-alpha in $POSTN^+$ SMCs potentially facilitated PAH progression. Furthermore, cell-cell interactions between $POSTN^+$ SMCs and regulator of G protein signaling-2 ($RGS2^+$) macrophages may participate in forming an inflammatory microenvironment.

Conclusions: Our study corroborated the correlation between POSTN and PAH through bioinformatics methods. It unveils that $POSTN^+$ SMCs and $RGS2^+$ macrophages form a mutually supportive and functionally significant interaction network, possibly playing a pivotal role in remodeling the extracellular matrix and promoting an inflammatory environment in PAH. These findings offer novel insights into PAH pathogenesis.

Keywords: pulmonary arterial hypertension; POSTN; fibroblasts; smooth muscle cells; macrophages; inflammatory microenvironment

Introduction

Pulmonary hypertension (PH) poses a significant global health concern, affecting approximately 1% of the world's population [1]. It is primarily characterized by elevated pulmonary artery pressure and right ventricular dysfunction, culminating in heart failure and death [1]. Individuals with PH typically exhibit a mean pulmonary artery pressure exceeding 20 mmHg. PH is classified into five clinical groups based on its pathophysiology, hemodynamics, clinical presentation, and therapeutic approaches [1,2]. Notably, group 1 PH, known as pulmonary arterial hypertension (PAH), is the most prevalent subtype.

The pathological hallmarks of PAH include progressive pulmonary vascular remodeling and elevated pulmonary vascular resistance, attributed to the proliferation and migration of smooth muscle cells (SMCs), endothelial cell dysfunction, and fibroblast activation [3,4]. Periostin (POSTN), a matricellular protein, participates in cell migration, adhesion, and epithelial-mesenchymal transition while also interacting with various extracellular matrix (ECM) proteins [5–7]. Recent studies have revealed the function

Journal of
BIOLOGICAL REGULATORS
and Homeostatic Agents

of POSTN in cardiovascular diseases. For example, reducing POSTN-expressing ($POSTN^+$) myofibroblasts attenuates collagen production and scar post-myocardial infarction [8,9]. Additionally, POSTN-traced myofibroblasts tend to transition to a low-activation state following lesion resolution [8,9]. Moreover, exposure of pulmonary arterial smooth muscle cells (PASMCs) to cigarette smoke extract, a recognized risk factor for PAH, leads to upregulation of POSTN expression [10].

This study employed bioinformatics and experimental methods to explore the association between POSTN and PAH. Additionally, at the single-cell level, we elucidated the dynamic evolution of fibroblasts and SMCs, shedding light on the potential mechanisms through which $POSTN^+$ SMCs regulate the immune microenvironment of PAH. Our findings offer novel insights into PAH pathogenesis.

Methods

Data Acquisition

GSE113439, GSE15197, and GSE117261 were downloaded from Gene Expression Omnibus (GEO) (https://www.ncbi.nlm.nih.gov/geo/). These datasets, comprising freely accessible gene expression microarray data, were extracted for analysis. The single-cell RNA sequencing (scRNA-seq) dataset, GSE210248, was also retrieved from GEO.

Integration of Gene Expression Microarray Datasets

Three microarray-based studies on PAH, available in the GEO database, were downloaded and normalized to create a meta-cohort. The Combat function within the Sva package (version 3.44.0, Johns Hopkins University, Baltimore, MD, USA) was employed to mitigate batch effects across the cohorts.

Differential Gene Expression Analysis

Differential mRNA expression was conducted using the limma package (version 4.2.2, The University of Melbourne, Melbourne, Australia). The screening criteria for differentially expressed mRNAs were $|\log_2 (\text{fold change})| \geq 1$ and $p < 0.05$.

Key Hub Gene Identification

The STRING database (https://cn.string-db.org/) was employed to construct protein-protein interaction networks based on eight upregulated genes in PAH. Subsequently, the generated network was imported into Cytoscape software (version 3.8.2, Institute for Systems Biology, Washington, WA, USA). Hub genes were then identified from the protein-protein networks using the Maximal Clique Centrality (MCC) algorithm implemented in Cytohubba.

Kyoto Encyclopedia of Genes and Genomes (KEGG) Functional Enrichment Analysis and Gene Set Enrichment Analysis (GSEA)

ClusterProfiler package (version 4.2.2, Southern Medical University, Guangzhou, China) in R was employed to conduct KEGG analysis and GSEA of differentially expressed gene sets. Following false discovery rate (FDR) correction, activated pathways were identified using the criteria NES > 0 and a significance p-value < 0.05. The GseaVis package (version 0.0.1, Southern Medical University, Guangzhou, China) in R was used for visualization.

Analysis of Immune Infiltration Using the MCP-Counter Algorithm

The MCP-counter algorithm (version 1.2.0, Université Paris Descartes, Paris, France) was utilized to quantify the abundance of 10 types of immune cells. Differences were analyzed using the Wilcoxon rank-sum test.

Single-Cell Transcriptomic and Differential Expression Analyses

Reads were aligned, and gene expression was quantified using CellRanger software (version 6.0.2, 10X genomics, California, CA, USA). Subsequent analysis was performed using the Seurat package (version 4.1.1, New York University, New York, NY, USA). Cells with fewer than 1000 unique molecular identifiers or more than 15% mitochondrial genes were excluded. Doublets were detected in each sample using DoubletFinder software (version 2.0.3, University of California, San Diego, CA, USA). Harmony algorithm was employed to mitigate batch effects. The top 4000 most variable genes, determined by the FindVariableFeatures function within Seurat package, were used for data scaling. Principal component analysis was carried out based on these variable genes. Additionally, using the top 50 principal components, FindNeighbors function within Seurat package was used to identify nearest neighbors for graph clustering. Cell subtypes were identified using FindCluster function within Seurat package. The Uniform Manifold Approximation and Projection (UMAP) algorithm was utilized to visualize cell distributions. Differentially expressed genes between clusters were determined using the "FindAllMarkers" function, with parameters set as follows: min.pct = 0.15, logfc.threshold = 0.15, and only.pos = T. p-values and adjusted p-values were obtained using the Wilcoxon rank-sum test with the Benjamini-Hochberg method.

Trajectory Analysis

Cellular differentiation based on the top 100 differentially expressed genes between cell subtypes was characterized using the Monocle2 algorithm (version 2.24.1, University of California, San Diego, CA, USA). Dimension reduction was performed using the reduceDimension function and the DDRtree reduction method, allow-

ing for a maximum of two components. Gene expression analysis based on branching fate was conducted using branch expression analysis modeling (BEAM). The plot_genes_branched_pseudotime function was utilized to visualize the expression of branch-specific genes along trajectories, with curves representing LOESS-smoothed gene expression across each trajectory.

Analysis of Transcription Factor (TF) Regulon

The regulatory network and activity of the regulon were analyzed using pySCENIC. Subgroup-specific TFs were identified using the Wilcoxon rank-sum test within pySCENIC. Additionally, the regulon-associated specific score (RSS) for each cell type was calculated based on the Jensen-Shannon divergence, computed using the philentropy package (version 0.6.0, University of Auckland, Auckland, New Zealand).

Gene Set Level Analysis for scRNA-seq Data

The run AUCell function in the pochi R package (version 0.1.0, New York University, New York, NY, USA) was utilized to score single-cell signatures. The two-sided Wilcoxon rank-sum test with Benjamini-Hochberg FDR correction was used to calculate enrichment scores for differential signatures between groups.

Cell-Cell Communications

Cell-cell communication was analyzed using CellPhoneDB Python (version 2.1.1, University of Toronto, Toronto, Canada) to elucidate potential interactions between different cell types in PAH as previously described [11]. CellPhoneDB Python package is a freely accessible repository containing curated ligands, receptors, and their interactions. The expressions of receptors in one cell type and corresponding ligands in another cell type were used to predict enriched receptor-ligand pairs between cell types. For subsequent analyses, receptors and ligands expressed in approximately 10% of cells within a specific cell type were considered, with significant pairs defined with a p-value < 0.05 and a mean value ≥ 1.

The Nichenet package was used to identify interactions between $POSTN^+$ SMCs and regulator of G protein signaling-2 ($RGS2^+$) macrophages (Mphs) to further elucidate the key mediators between two cell subgroups. For ligand-receptor interactions, genes expressed in more than 10% of cell clusters were considered. The top 20 ligands and 100 targets of differentially expressed genes in "sender cells" and "receive cells" were analyzed to assess paired ligand-receptor activity. The regulatory activity of ligands was visualized using the Nichenet_output$ligand_activity_target_heatmap, with activity scores ranging from 0 to 1. Finally, average gene expression in the specified cell types was measured and scaled across indicated subtypes to illustrate the expression of differentially expressed ligands and receptors in the heatmap.

Deconvolution of Cell Types for the RNA-seq Datasets

To assess the function of the cell types in a large compendium of samples, CIBERSORTx was used to generate a reference signature matrix from our scRNA-seq dataset and predict the proportion of the cell types from the integrated microarray dataset based on the constructed references of the cell types. Quartile normalization was applied to the microarray datasets within CIBERSORTx, with default settings for all other parameters.

The integrated microarray dataset was subjected to quartile normalization to estimate cell fractions. The permutation parameter was 100 iterations, while default settings were used for other parameters. Spearman's correlation analysis was conducted to elucidate relationship among the proportions of infiltrated cell types. Graphs were generated using the corrplot package (version 0.92, Capital One, McLean, VA, USA).

Animal Experiments

Pulmonary arterial hypertension (PAH) model tissues were obtained from the Department of Forensic Medicine, Nanjing Medical University. Briefly, twelve male Sprague Dawley rats (Charles River), approximately 6 weeks old and weighing 200–250 g, were procured from Vital River Biological Co., Ltd. (Beijing, China). The rats were randomly divided into control (n = 6) and monocrotaline (MCT) (n = 6) groups.

Following established protocols [12], rats in the MCT group received intraperitoneal injections of 60 mg/kg monocrotaline (cat. no C2401, Sigma-Aldrich, St. Louis, MO, USA) and were housed for 4 weeks. Conversely, rats in the control group received an equivalent volume of saline via intraperitoneal injection and were housed for 4 weeks. Male C57BL/6 mice aged 6–8 weeks were utilized for the PAH mouse model. SU5416 (cat. no S8442, Sigma-Aldrich, St. Louis, MO, USA) was subcutaneously injected at a dose of 20 mg/kg weekly, followed by exposure to chronic hypoxia (10% O_2, 90% N_2) in a ventilated chamber for 4 weeks (Su/Hx group, n = 6) [13]. The control group (normoxia group, n = 6) received vehicle injections and was housed under normoxic conditions.

After measuring right ventricular pressure, rats were euthanized under anesthesia by excess CO_2, and their pulmonary circulatory system was flushed with sterile phosphate-buffered saline (PBS) at 4 °C. The hearts were dissected to isolate the right ventricular free wall. Right ventricular hypertrophy was assessed by calculating the Fulton index, defined as the weight of the right ventricle to the weight of the left ventricle and septum [14]. Lung tissue samples were collected for further analysis, including hemodynamic and histological examination, to confirm the successful construction of the model. These results were corroborated by the Department of Forensic Medicine.

Journal of
BIOLOGICAL REGULATORS
and Homeostatic Agents

Animals were housed under a 12-hour light/dark cycle and provided standard food and water ad libitum. All animal experiments were approved by the Committee on the Ethics of Animal Experiments of Nanjing Medical University (approval number: IACUC-2001008) and conducted according to the Guide for the Care and Use of Laboratory Animals.

Western Blot Analysis

Lung tissues and pulmonary arterial smooth muscle cells (PASMCs) were lysed using RIPA buffer (Cat. No KGP702, Keygen Biotech. Co., Ltd., Nanjing, China) supplemented with 1% protease inhibitor cocktail and 1% phenylmethylsulfonyl fluoride. Subsequently, the lysates were centrifuged at 4 °C and 13,000 rpm for 15 minutes, and protein supernatants were collected and quantified using the BCA Protein Assay Kit (T9300A, TaKaRa, Osaka, Japan).

Proteins were separated by sodium dodecyl sulfate-polyacrylamide gel electrophoresis (SDS-PAGE), followed by transfer onto polyvinylidene fluoride (PVDF) membranes (Millipore), which were then blocked with 5% BSA. Membranes were incubated overnight at 4 °C with primary antibodies against POSTN (Proteintech, 1:2500 dilution) and β-actin (Cell Signaling Technology, 1:1000 dilution), followed by incubation with horseradish peroxidase-conjugated secondary antibody (Fdbio science, 1:8000 dilution) at room temperature for 2 hours. Subsequently, sample detection was performed using an enhanced chemiluminescence (ECL) reagent (NCM biotech), and blots were quantified using ImageJ software (version 1.8.0, University of Wisconsin Optical and Computational Instrumentation Laboratory, Madison, WI, USA).

Statistical Analysis

Statistical analyses were conducted using R software (version 4.1.0, New York University, New York, NY, USA). Differences between the two groups were assessed using the Wilcoxon rank-sum test. Multiple hypotheses were calibrated via the Bonferroni method. Pearson's correlation test was used to measure the linear correlation between two variables. A significance threshold of $p < 0.05$ was considered statistically significant. Statistics significant levels were denoted as follows: $*p < 0.05$, $**p < 0.01$, $***p < 0.001$, and $****p < 0.0001$. The term "ns" indicated the absence of statistical significance ($p > 0.05$).

Results

POSTN as a Biomarker for PAH

To identify the potential biomarkers for PAH, the Combat algorithm was used to integrate three PAH expression profiling microarray datasets without bias (Fig. 1A). Differential expression analysis, combined with stringent filtering criteria, revealed eight significantly upregulated genes (*COL14A1, HBB, POSTN, HBA2, PI15, SFRP2, VCAM1,* and *ASPN*) and nine significantly downregulated genes (*RNASE2, S100A9, MGAM, SOSTDC1, S100A8, S100A12, IL1R2, BPIFB1,* and *BPIFA1*) (Fig. 1B,C). Further exploration of the protein interaction network imputed in STRING, combined with the CytoHubba algorithm, identified POSTN as the top hub gene among the upregulated genes (Fig. 1D). Notably, POSTN is an ECM protein involved in injury-induced tissue remodeling and PAH pathogenesis.

Five-fold cross-validation of independent POSTN expression facilitated PAH diagnosis, achieving an area under the curve (AUC) of 0.8 (Fig. 1E). Based on POSTN expression levels, PAH samples were classified into two groups: low and high POSTN expression. The high POSTN expression group correlated with ECM, exhibiting increased expression of collagen family genes (*COL1A1, COL14A1,* and *COL3A1*), *VCAM1, ASPN,* and *PI15*. Conversely, *SOST, MS4A15, GPR78, FCN3,* and *SLC6A4* were elevated in the low POSTN expression group (Fig. 1F).

Differentially expressed genes in the high and low POSTN expression groups were subjected to gene functional enrichment analysis to elucidate the molecular mechanisms underlying POSTN in PAH. In the high POSTN expression group, upregulated genes were enriched in ECM-associated pathways, including the phosphatidylinositol 3-kinase (PI3K)/protein kinase B (AKT) signaling pathway, focal adhesion, protein digestion and absorption, MAPK signaling, and Rap1 signaling. Conversely, in the low POSTN expression group, upregulated genes were enriched in pathways associated with the synthesis, secretion, and action of parathyroid hormone, the transforming growth factor beta (TGF-β) signaling pathway, nitrogen metabolism, neuroactive ligand-receptor interaction, and proximal tubule bicarbonate reclamation (Fig. 1G). These findings underscore the association between POSTN and ECM remodeling, positioning it as a functional target for PAH. Moreover, to elucidate the correlation between POSTN and PAH, POSTN expression was measured in the rat MCT-PAH and mouse Su/Hx-PAH models, revealing a significant upregulation in PAH animal models compared to the control group (Fig. 1H, $p < 0.001$).

Association of POSTN with Fibroblast Infiltration in PAH

Accumulating evidence underscores the significant influence of POSTN on immune response regulation [15]. We investigated the microenvironment composition of the low and high POSTN expression groups. Overall, compared to the low POSTN expression group, the high POSTN expression group exhibited a higher stromal score ($p < 0.01$) and lower immune score ($p < 0.0001$) (Fig. 2A). Subsequently, employing the MCP-counter approach, we assessed variations in immune infiltration of 10 types of immune cells between the two groups. Notably, the proportion of fi-

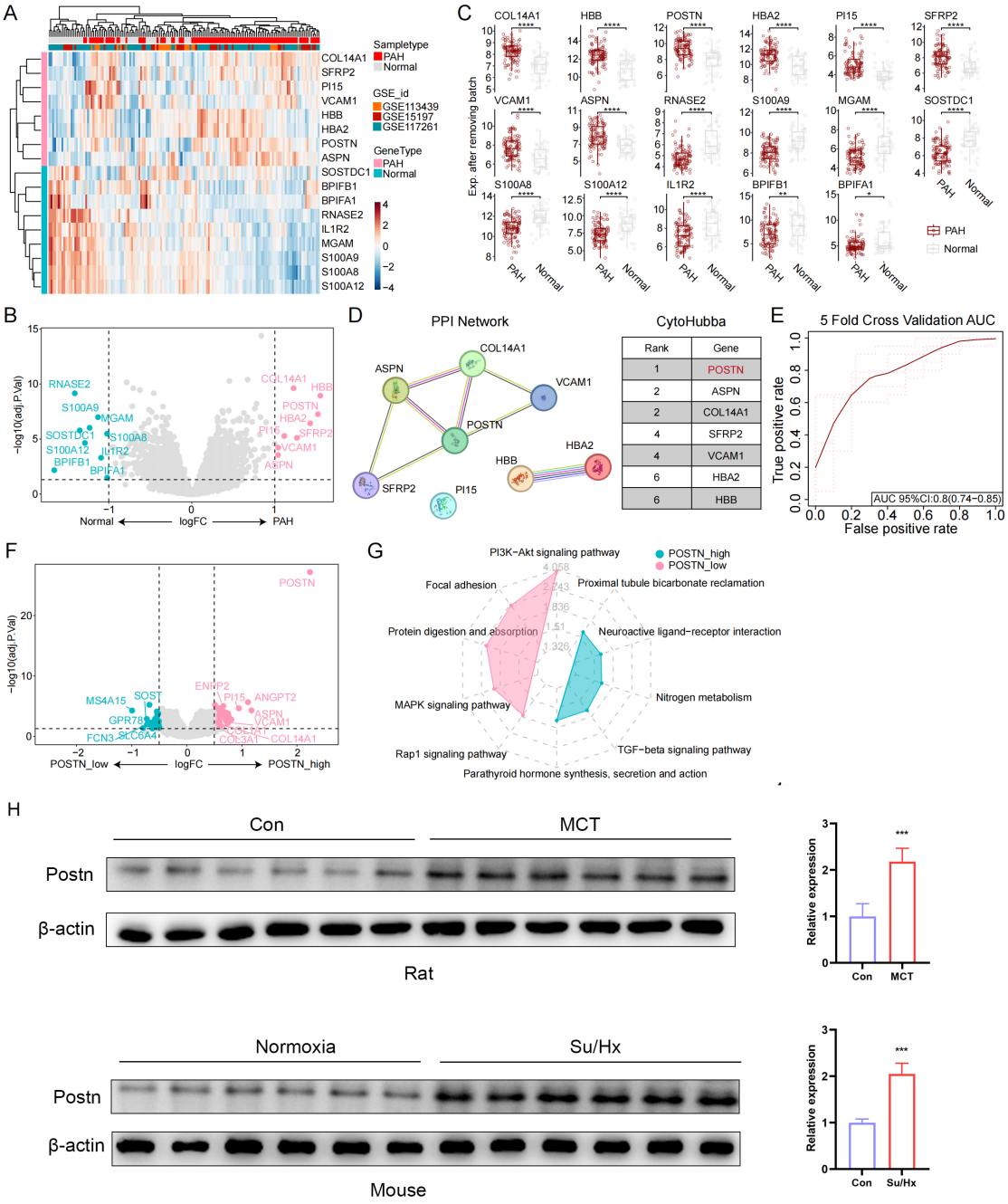

Fig. 1. Identification of a potential pulmonary arterial hypertension (PAH) biomarker. (A) Heatmap illustrating the differentially expressed genes in samples annotated based on sample types and corresponding GSE numbers. The color scale ranges from blue, indicating low gene expression, and red, indicating high gene expression. (B) Analysis of differentially expressed genes between PAH and normal samples. Pink indicates PAH samples, while blue represents normal samples. (C) Box plots showing the expression levels of eight significantly upregulated genes (*COL14A1, HBB, POSTN, HBA2, PI15, SFRP2, VCAM1,* and *ASPN*) and nine significantly downregulated genes (*RNASE2, S100A9, MGAM, SOSTDC1, S100A8, S100A12, IL1R2, BPIFB1*, and *BPIFA1*). Different colors indicate different sample types. (D) Left: Protein-protein interaction network of the eight significantly upregulated genes from STRING (https://cn.string-db.org/). Right: The Maximal Clique Centrality (MCC) algorithm in CytoHubba ranked the eight significantly upregulated genes, with the top gene marked in red. (E) Area under the curve (AUC) for the five-fold cross-validation of the integrated microarray dataset. The red line represents the mean AUC value. (F) Analysis of differentially expressed genes between samples with high and low periostin (POSTN) expression. Pink indicates samples with high POSTN expression, while blue indicates low POSTN expression. (G) Radar plot depicting the functional enrichment results of the high (pink) and low (blue) POSTN expression groups. (H) Western blotting of the POSTN protein in lung tissues from Su/Hx-PAH mice (mice: normoxia, n = 6, Su/Hx, n = 6) and monocrotaline (MCT)-induced PAH rats (rats: control, n = 6, MCT, n = 6). *$p < 0.05$, **$p < 0.01$, ***$p < 0.001$, and ****$p < 0.0001$.

Journal of
BIOLOGICAL REGULATORS
and Homeostatic Agents

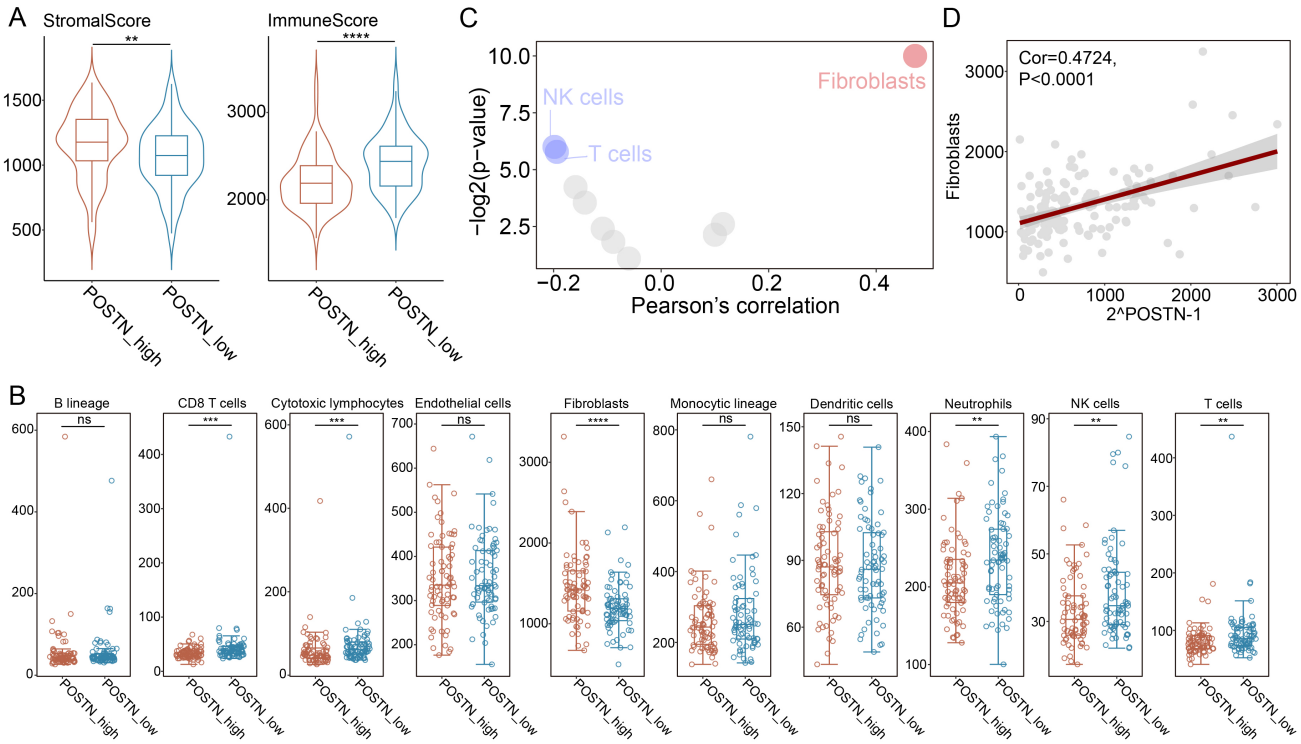

Fig. 2. Immune infiltration analysis. (A) Box plots depicting the stromal (left) and immune (right) scores of the high (red) and low (blue) POSTN expression groups. (B) Box plots illustrating the infiltration levels of 10 cell types in the high (red) and low (blue) POSTN expression groups. Differences were evaluated using the Wilcoxon rank-sum test. (C) Scatter plot showing the correlation between POSTN expression and the infiltration levels of 10 cell types. (D) Correlation between fibroblast infiltration and POSTN expression. Correlation analysis was conducted using Pearson's correlation test. ns $p > 0.05$, **$p < 0.01$, ***$p < 0.001$, and ****$p < 0.0001$.

broblasts was significantly elevated in patients with high POSTN expression compared to those with low POSTN expression ($p < 0.001$). Conversely, immune cell infiltration, including $CD8^+$ T cells ($p < 0.001$), cytotoxic lymphocytes ($p < 0.001$), neutrophils ($p < 0.01$), natural killer (NK) cells ($p < 0.01$), and T cells ($p < 0.01$), was more abundant in patients with low POSTN expression relative to those with high POSTN expression (Fig. 2B).

Moreover, we elucidated the correlation between POSTN expression and the infiltration of 10 cell types. Interestingly, fibroblast infiltration positively correlated with POSTN expression in PAH (Fig. 2C,D, Pearson's correlation test, rho = 0.4724, $p < 0.001$). However, NK and T cell infiltration exhibited a significant negative correlation with POSTN expression in PAH (Fig. 2C). Collectively, these findings suggest an elevation in fibroblast infiltration among patients with high POSTN expression.

Identification of $POSTN^+$ SMCs in PAH

The scRNA-seq dataset of human pulmonary arteries, comprising three healthy individuals and three participants with PH, was reanalyzed to comprehensively determine the cellular composition of the PAH microenvironment, as presented by Crnkovic *et al.* [16]. The Harmony algorithm was employed to mitigate batch effects in the scRNA-seq dataset (Fig. 3A). Following quality control, 22,625 cell transcriptomes were retained for subsequent analysis. These transcriptomes were then clustered into 33 distinct clusters representing 14 cell subtypes (Fig. 3A). These subtypes were identified based on traditional single-cell marker expression and comprised B cells (MS4A1 and CD79A), dendritic cells (DCs) (FCER1A and CLEC10A), endothelial cells (CLDN5 and VMF), epithelial cells (KRT8 and KRT19), fibroblasts (DCN and COL1A2), granulocytes (S100A8 and S100A9), mast cells (CPA3 and KIT), macrophages/monocytes (Mph/Mono) (C1QB and C1QA), NK cells (GNLY and GZMB), plasma cells (MZB1 and IGKC), proliferative cells (STMN1 and MKI67), smooth muscle cells (SMCs) (ACTA2 and TAGLN), T cells (CD3D and CD3E), and regulatory T cells (Tregs) (FOXP3 and CTLA4) (Fig. 3C). We compared the infiltration of these cell subtypes across different sample types and revealed significant variations in immune cell composition. Notably, immune cells such as B cells, T cells, NK cells, DCs, mast cells, and Tregs were enriched in PAH samples, accompanied by a decrease in normal samples (Fig. 3B). These findings are consistent with previous study and underscore the pivotal role of dynamic changes in immune and stromal cells in PAH progression [17].

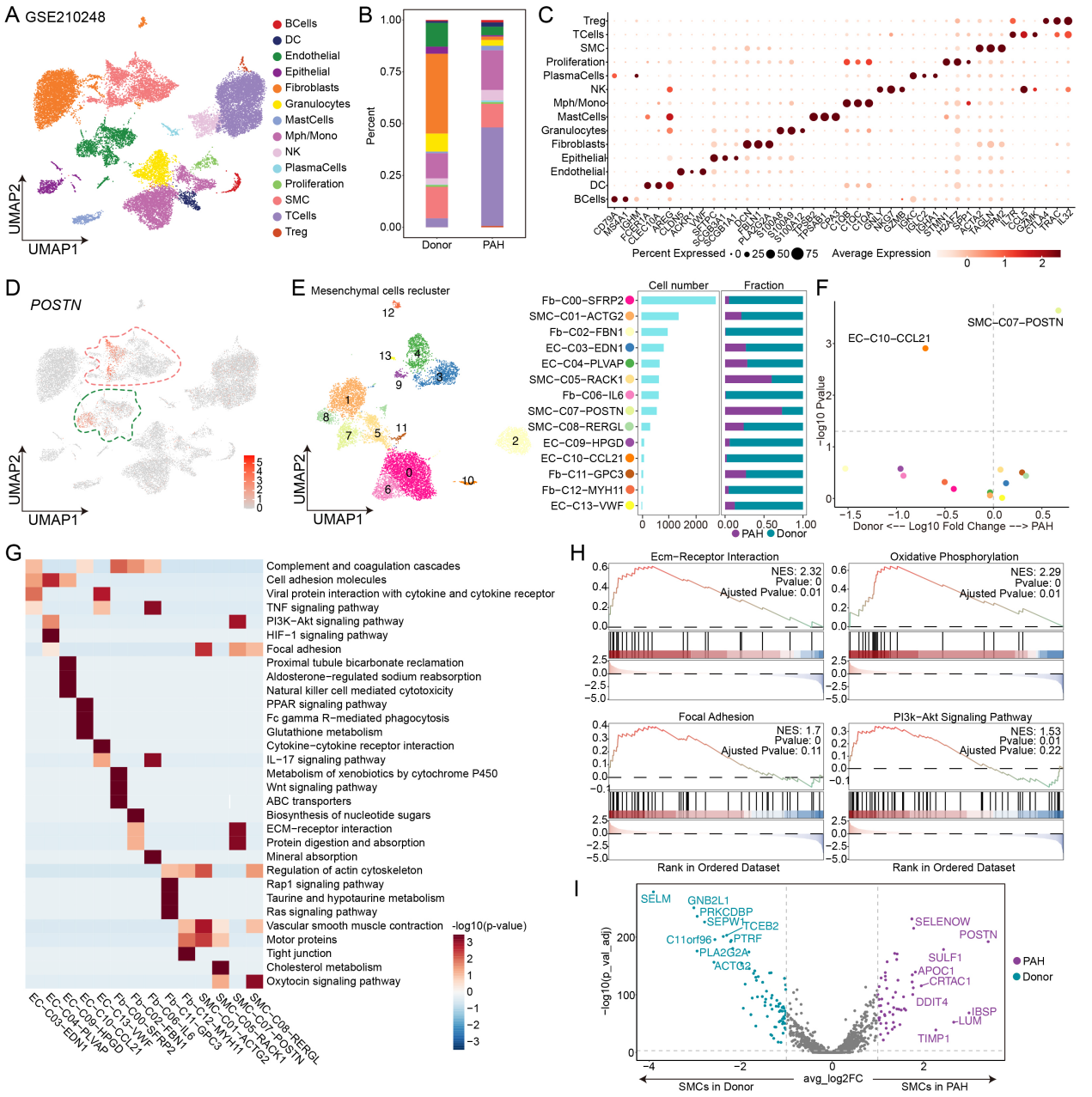

Fig. 3. Single-cell RNA sequencing (scRNA-seq) analysis. (A) Uniform Manifold Approximation and Projection (UMAP) plot classifying cell types. Different colors represent different cell types, including dendritic cells (DCs), macrophages/monocytes (Mph/Mono), natural killer (NK) cells, and smooth muscle cells (SMCs). (B) Bar plot indicating the abundance of cell types across different sample types. Different colors represent different cell types. (C) Dot plot displaying the top three differentially expressed genes of each cell type. Color depth indicates the average expression value, while the point size indicates the gene expression percentage. (D) UMAP plot illustrating POSTN expression. Different colored circles indicate the two cell types with significant POSTN expression. (E) Left: UMAP plot highlighting the cluster of mesenchymal cells. Different colors represent different cell subtypes. Middle: Bar plots showing the cell numbers in each cluster. Right: Bar plots indicating the proportion of the sample types in each cluster. Different colors denote different sample types. (F) Scatter plot highlighting the enrichment of each cluster in different sample types using a beta-binomial generalized linear model. Different colors represent different cell subtypes. (G) Kyoto Encyclopedia of Genes and Genomes (KEGG) terms of the differentially expressed genes significantly enriched in each mesenchymal cell subtype. Colors denote the scaled value of the -$\log_{10}$ p-value. (H) Gene set enrichment analysis (GSEA) of extracellular matrix (ECM)-receptor interaction, phosphatidylinositol 3-kinase (PI3K)/protein kinase B (AKT) signaling, focal adhesion, and oxidative phosphorylation between POSTN^{+} SMCs and other SMCs. Genes were ranked based on fold changes in expression between these two conditions. (I) Analysis of differentially expressed genes between the SMCs in PAH and normal samples. Purple indicates PAH samples, while cyan represents normal samples.

Journal of
BIOLOGICAL REGULATORS
and Homeostatic Agents

Furthermore, POSTN expression was determined in the scRNA-seq dataset, revealing its clustering in fibroblasts and SMCs (Fig. 3D). Subsequently, mesenchymal cells were reclustered into 14 clusters, encompassing five fibroblast clusters (Fb-C00-SFRP2, Fb-C02-FBN1, Fb-C06-IL6, Fb-C11-GPC3, and Fb-C12-MYH11), four SMC clusters (SMC-C01-ACTG2, SMC-C05-RACK1, SMC-C07-POSTN, and SMC-C08-RERGL), and five endothelial cells (ECs) clusters (EC-C03-EDN1, EC-C04-PLVAP, EC-C09-HPGD, EC-C10-CCL21, and EC-C13-VWF). Compared with normal tissues, PAH tissues were significantly enriched with SMC-C07-POSTN and SMC-C05-RACK1 (Fig. 3E). After analyzing changes in cell abundance, differential composition analysis, employing a beta-binomial generalized linear model, revealed significant enrichment of SMC-C07-POSTN in PAH (Fig. 3F). KEGG functional enrichment analysis of distinct mesenchymal subpopulations revealed notable enrichment of ECM-receptor interaction, PI3K-AKT signaling, protein digestion and absorption, and focal adhesion in SMC-C07-POSTN (Fig. 3G). Furthermore, GSEA revealed that compared with the other SMCs, ECM-receptor interaction ($p < 0.001$), PI3K-AKT signaling ($p = 0.01$), focal adhesion ($p < 0.001$), and oxidative phosphorylation ($p < 0.001$) were significantly enriched in SMC-C07-POSTN (Fig. 3H). Interestingly, various cell subpopulations exhibited distinct metabolic activation characteristics, including upregulated glutathione metabolism in EC-C10-CCL21, enriched cholesterol metabolism in SMC-C05-RACK1, and upregulated xenobiotic metabolism by cytochrome P450 in Fb-C00-SFRP2 (Fig. 3G). Notably, POSTN emerged as the top differentially expressed gene between SMCs in PAH and donors, suggesting the specific enrichment of ECM modeling-associated POSTN$^+$ SMCs in the PAH microenvironment (Fig. 3I).

Cell-State Transition Trajectory of Different SMC Subpopulations in PAH

The Monocle 2 algorithm was used to establish a pseudotime cell trajectory, allowing for the elucidation of dynamic processes within fibroblasts and SMCs at the single-cell level (Fig. 4A). Notably, the integration of pseudotime and inferred state statistical analyses revealed two distinct trajectories; where Fb-C00-SFRP2 occupied the progenitor state and subsequently branched into SMC-C07-POSTN and SMC-C01-ACTG2 (Fig. 4A–D). The differentiation branch leading to POSTN$^+$ SMC was notably enriched with PAH cells (Fig. 4C). Additionally, most fibroblast subtypes were observed in the progenitor and initiation state (Fig. 4D). Subsequently, gene expression patterns associated with the two differentiation branches involved in SMC state transitions were explored. Through a smoothed heatmap, the highly expressed genes in the early trajectory stage were functionally enriched (cluster 4) in both differentiation branches, with enrichment in processes such as epithelial-mesenchymal transition, myogenesis, apical junction, and oxidative phosphorylation (Fig. 4E). In contrast to the SMC-C01-ACTG2 differentiation branch, the expressions of cluster 3 genes, implicated in tumor necrosis factor-alpha signaling via the NF-κB pathway, epithelial-mesenchymal transition, apoptosis, and disease progression-associated hypoxic pathways, were higher in the terminal state of the SMC-C07-POSTN differentiation branch (Fig. 4E). Furthermore, the expression of cluster 1 genes, enriched in processes such as epithelial-mesenchymal transition, angiogenesis, interferon-gamma responses, and the interferon-alpha response pathway, increased in the terminal state of the SMC-C01-ACTG2 differentiation branch (Fig. 4E). Given the critical role of hypoxia in PAH and its impact on SMC heterogeneity, BEAM analysis was performed to identify potential differentially expressed genes between the two branches. The expressions of ECM-related features (*COL1A1, COL3A1, THBS2, CTHRC1, FN1, VCAN,* and *TGM2*) and hypoxia-associated features (*SERPINE1, SERPINE2,* and *CD9*) were upregulated in the POSTN$^+$ SMC differentiation branch, indicating that hypoxia stimulates SMC-mediated collagen secretion to modulate the ECM. Additionally, in the POSTN$^+$ SMC differentiation branch, *CXCL12* (a cytokine) and *SULF1* (an extracellular sulfatase) were significantly upregulated (Fig. 4F).

To identify the master regulator of POSTN$^+$ SMCs, pySCENIC was employed to evaluate the top transcription factors (TFs) that were specifically expressed and their corresponding activities in the TF regulatory network. Notably, within a hypoxic microenvironment, hypoxia-inducible factor 1-alpha (HIF1α) expression and activity were high in the regulatory network of POSTN$^+$ SMCs, suggesting its role as the key TF driving this differentiation pathway (Fig. 4G–I). Furthermore, the Jensen-Shannon divergence was used to calculate the regulon-associated specific score (RSS) of POSTN$^+$ SMCs. RSS identified HIF1α as one of the top 15 prevalent TFs (Fig. 4H). Collectively, these findings suggest that HIF1α activation in POSTN$^+$ SMCs drives PAH progression during hypoxia.

Cell-Cell Interaction of POSTN$^+$ SMCs and RGS2$^+$ Mphs Contributes to the Inflammatory Microenvironment

The cellphonedb method was employed to conduct cell-cell interaction analysis, investigating the interplay among major cell types to elucidate the mechanisms governing the regulation of the PAH immune microenvironment by POSTN$^+$ SMCs. Compared to normal donors, PAH samples exhibited a strong interaction between SMCs and macrophages/monocytes (Mph/Mono) (Fig. 5A), suggesting that POSTN$^+$ SMCs contribute to an inflammatory microenvironment by influencing Mph/Mono. Based on the expression of specific marker genes, seven subtypes were identified in the Mph/Mono lineage: six

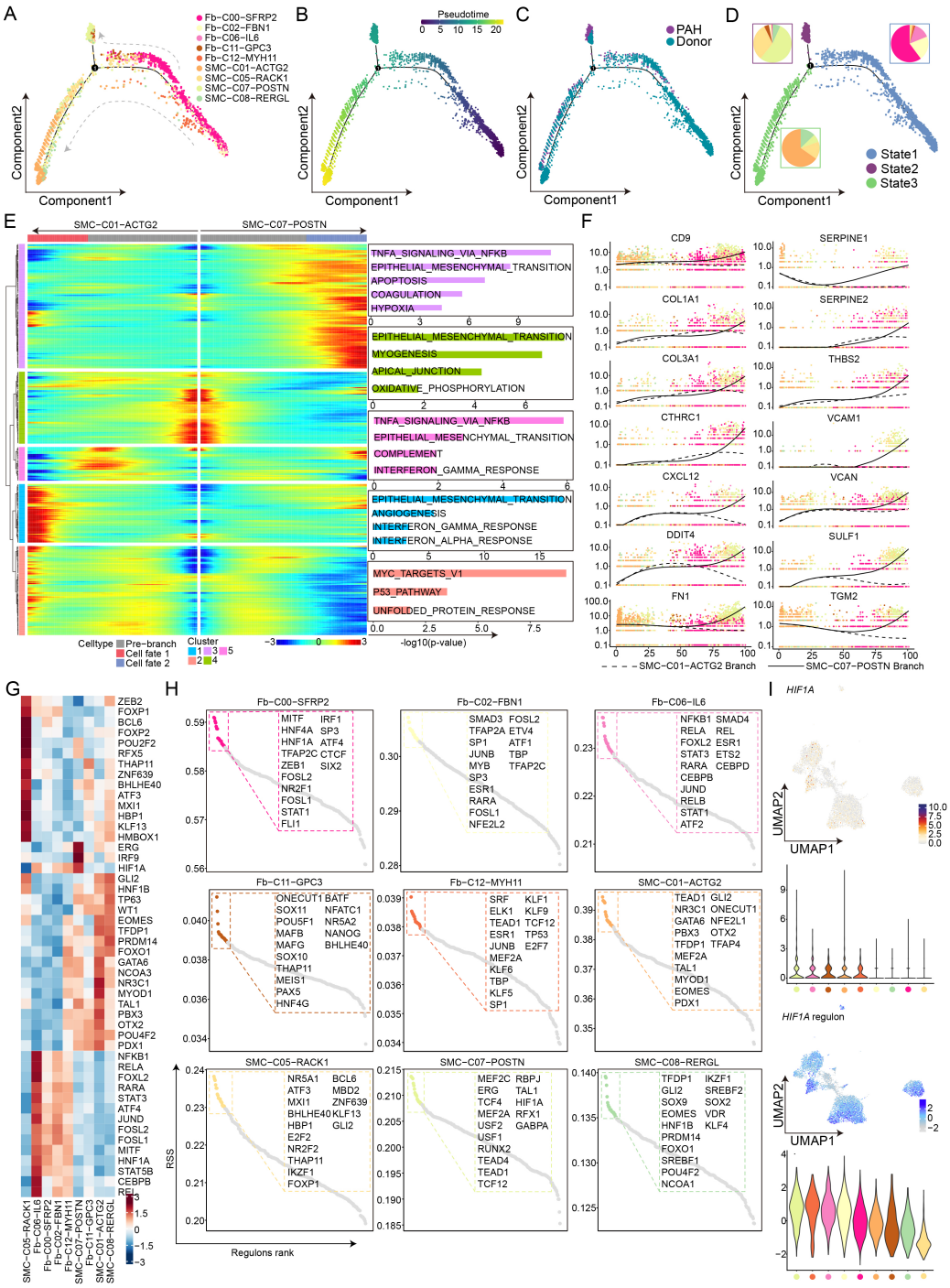

Fig. 4. Trajectory analysis of fibroblast and SMC subtypes. (A) Developmental trajectory of fibroblasts and SMCs was inferred using monocle 2 and colored based on the subtypes. (B) Pseudotime of the developmental trajectory. Colors from purple to yellow indicate low to high values. (C) Sample types of developmental trajectories are colored based on sample types. (D) Inferred states of the trajectory. Proportions of the cell subtypes are depicted in the circles, with each colored circle representing a different state. (E) Expression heatmap showing significant ($q < 1 \times 10^{-3}$) genes identified via branch expression analysis to compare the fate of two SMC cells (left). Box plots highlighting the top significantly enriched hallmark pathways in each gene cluster (right). (F) Pseudotime projections of the transcriptional changes in genes associated with the extracellular matrix and hypoxia between two trajectory branches. (G) Heatmap depicting the mean activity of the top differentially activated regulons in each fibroblast and SMC subtype inferred using pySCENIC. (H) Dot plots highlighting the top 15 specifically activated transcription factors (TFs) ranked based on their regulon-associated specific score (RSS) in each fibroblast and SMC subtype. (I) Up: UMAP and violin plots illustrating hypoxia-inducible factor 1-alpha (HIF1α) expression. Bottom: UMAP and violin plots depicting HIF1α regulon activity.

Journal of
BIOLOGICAL REGULATORS
and Homeostatic Agents

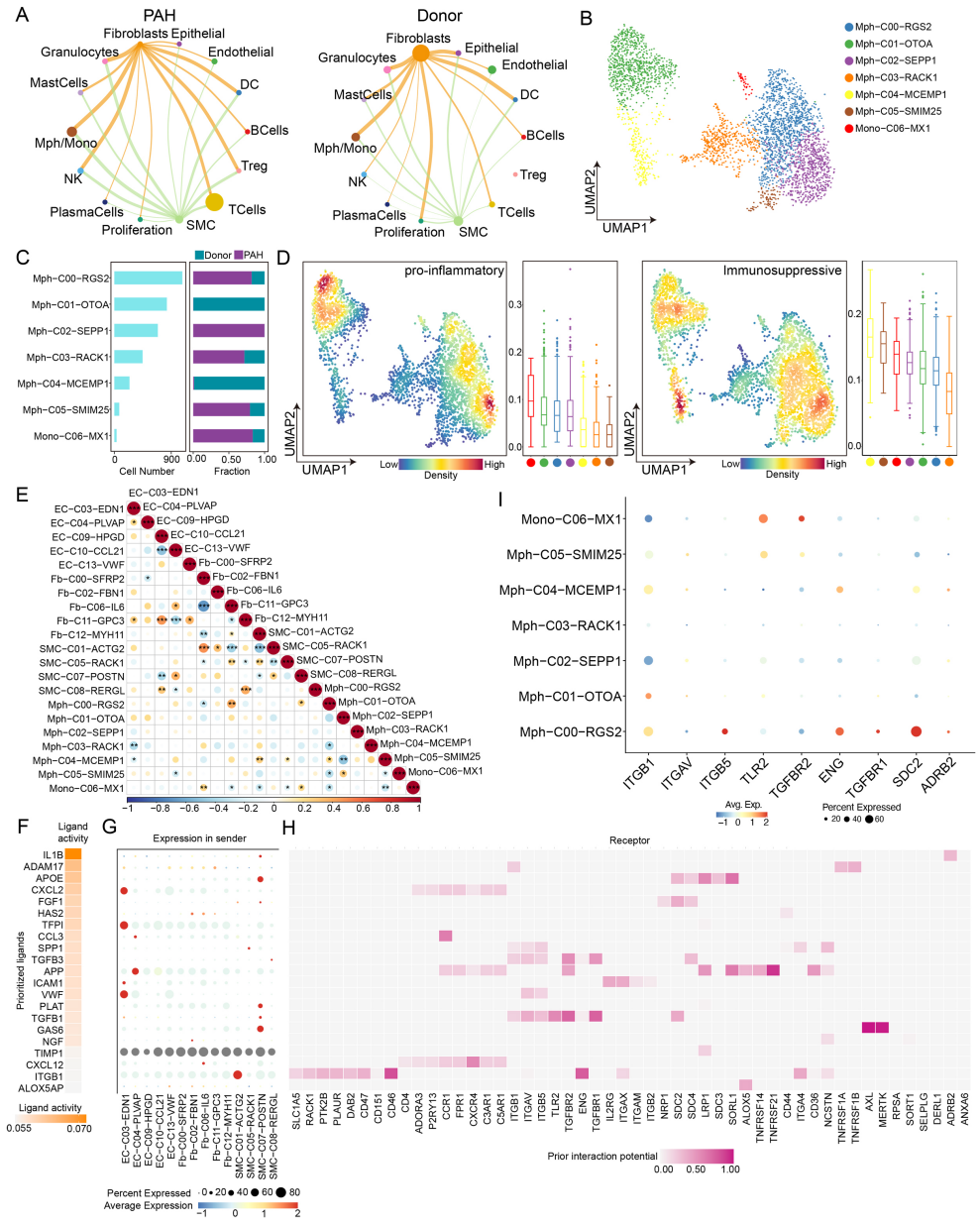

Fig. 5. Characterization of macrophages in normal and PAH samples. (A) Chord diagrams illustrating cell-cell interactions among major cell types in PAH (left) and donor (right) samples. (B) UMAP plot of individual macrophages or monocytes. Each dot represents one cell, and color represents cell subtypes. (C) Left: Bar plots highlighting cell numbers in each cluster. Right: Bar plots highlighting the proportion of sample types in each cluster. Different colors denote different sample types. (D) UMAP plots illustrate the density distribution of proinflammatory and immunosuppressive scores. Corresponding box plots depict proinflammatory and immunosuppressive scores of each macrophage and monocyte subtype. Each dot represents one cell, and the color represents the cell subtypes. Red represents Mono-C06-MX1, green represents Mph-C01-OTOA, blue represents Mph-C00-RGS2, purple represents Mph-C02-SEPP1, yellow represents Mph-C04-MCEMP1, orange represents Mph-C03-RACK1, brown represents Mph-C05-SMIM25. (E) Dot plots depicting the Spearman's correlation for infiltration of pairwise fibroblast subtypes, SMC subtypes, and macrophage/monocyte subtypes in the integrated microarray cohort. Dot size and color denote Spearman's correlation, and black dots represent the significance at different p-value thresholds of $^{*}p < 0.05$, $^{**}p < 0.01$, $^{***}p < 0.001$. (F) NicheNet was utilized to infer the top-ranked ligands regulating RGS2^{+} macrophages via POSTN^{+} SMCs. (G) Dot plots highlighting the expression percentage (dot size) and intensity (dot intensity) of top-ranked ligands (F) in each mesenchymal cell subtype. (H) Ligand-receptor pairs exhibiting interaction of RGS2^{+} macrophages with POSTN^{+} SMCs measured via ligand activity (F). (I) Dot plots depicting the expression percentage (dot size) and intensity (dot intensity) of interleukin 1 beta (*IL1β*)- gene or transforming growth factor beta 1 (TGFβ1)-targeted receptors in each mesenchymal cell subtype. RGS2^{+}, regulator of G protein signaling-2.

macrophages (Mph-C00-RGS2, Mph-C01-OTOA, Mph-C02-SEPP1, Mph-C03-RACK1, Mph-C04-MCEMP1, and Mph-C05-SMIM25) and one monocyte (Mono-C06-MX1) (Fig. 5B). Notably, in PAH, Mph-C00-RGS2, Mph-C02-SEPP1, Mph-C05-SMIM25, and Mono-C06-MX1 were predominantly enriched (Fig. 5C). Subsequently, we computed the enriched scores for proinflammatory and immunosuppressive cells, revealing a higher prevalence of proinflammatory responses in RGS2$^+$ Mphs (Fig. 5D). To assess the infiltration patterns of these subtypes, we evaluated the infiltration of the 21 cell subtypes identified via single-cell RNA sequencing of the integrated microarray cohort using CIBERSORTx and calculated the pairwise Spearman correlations among these cell subtypes (Fig. 5E). Among the cell populations in the integrated microarray cohort, the highest correlation was observed between POSTN$^+$ SMCs and RGS2$^+$ Mphs (Fig. 5E).

To identify the key regulators of the interaction between POSTN$^+$ SMCs and RGS2$^+$ Mphs in PAH, the NicheNet package was used to elucidate the mechanisms underlying the interplay between these cell types. The activities of the ligands for interleukin 1 beta (IL1β), APOE, transforming growth factor beta 1 (TGFβ1), FGF1, and GAS6 were elevated in POSTN$^+$ SMCs, accompanied by relatively increased gene expression of *IL1β, APOE, TGFβ1, FGF1,* and *GAS6* (Fig. 5F,G). Furthermore, the protein encoded by TGFβ1 bound to the receptors ITGB5, ENG, TGFBR1, and SDC2 expressed on RGS2$^+$ Mphs, while the protein encoded by IL1β bound to the ADRB2 receptor expressed on RGS2$^+$ Mphs (Fig. 5H,I). These findings suggest that POSTN$^+$ SMCs regulate the formation of an inflammatory environment in RGS2$^+$ Mphs via the TGFβ1-SDC2 axis. Overall, our findings suggest the establishment of a mutually supportive and functionally significant interaction network between POSTN$^+$ SMCs and RGS2$^+$ Mphs, which may play vital roles in ECM remodeling and promotion of the inflammatory environment in PAH.

Discussion

Pulmonary arterial hypertension (PAH) is a progressive and fatal disease characterized by the obstruction of small pulmonary arteries due to endothelial dysfunction and uncontrolled proliferation of SMC and fibroblast within the pulmonary arteries [18,19]. Elevated pulmonary artery pressure, resulting from vascular obstruction, often leads to right ventricular failure with symptoms such as tachypnea and syncope. Despite the development of multiple pharmacological interventions targeting the endothelin, nitric oxide, and prostacyclin pathways in recent years, the prognosis for PAH patients remains unsatisfactory, imposing a significant burden on patients and physicians [20,21]. Therefore, there is an urgent need for further studies to elucidate PAH pathogenesis.

Periostin (POSTN), previously known as osteoblast-specific factor-2, belongs to the family of unstructured ECM proteins [22]. These proteins are highly expressed under pathological conditions such as inflammation, tissue repair, and trauma [23]. Studies have identified POSTN as a potential marker for various skeletal and non-skeletal disorders, including diabetes, allergy, asthma, and cancer [24–30]. POSTN impacts cell proliferation, migration, adhesion, and angiogenesis via cellular integrin receptors. Notably, POSTN is characterized by the presence of vitamin K-dependent γ-carboxyglutamate residues, which regulate the coagulation cascade [31]. Moreover, POSTN is upregulated in collagen-rich connective tissues subjected to mechanical stress or injury, such as the aorta, heart valves, bones, lungs, tendons, and skin [22]. As a multi-modular protein, POSTN interacts with or regulates other proteins, such as type I collagen, osteocalcin, and fibronectin, playing a vital role in collagen assembly, bone turnover, cardiovascular system regulation, and tissue cross-linking [32–34].

Several recent studies have highlighted the significance of POSTN in circulatory system disorders [6,10,35]. Studies focusing on PH revealed that POSTN expression was upregulated under hypoxic conditions in human and animal PH models, promoting its progression through a positive feedback loop involving HIF-1α and POSTN [35,36]. This suggests that targeting POSTN expression regulation may offer an effective therapeutic strategy for managing PH and serve as a valuable biomarker for assessing disease severity. In the present study, the Combat algorithm was used to unbiasedly integrate three PAH expression microarray datasets. Differential gene expression analysis was conducted using stringent filtering criteria, and protein interaction networks were explored using the CytoHubba algorithm. Among the upregulated genes, POSTN emerged as the top-ranked hub gene. Furthermore, POSTN expression was assessed in the monocrotaline-induced PAH rat and Sugen/hypoxia (Su/Hx) induced PAH mouse models. Compared with controls, POSTN expression was significantly increased in animal PAH models. Increasing evidence suggests that a complex interaction between immune and vascular stromal cells contributes to PAH pathogenesis [37,38]. In this study, we characterized the microenvironment composition in the high and low POSTN expression groups. Overall, the stromal score was higher, and the immune score was lower in the high POSTN expression group. Furthermore, immune cell enrichment was lower than that in the low POSTN expression group. Interestingly, a significant positive correlation was observed between fibroblast infiltration and POSTN expression in PAH.

The development of single-cell RNA sequencing (scRNA-seq) has facilitated comprehensive analysis of the disease microenvironment, enabling the identification of novel and unique immune cell subsets in health and disease, determining stochastic heterogeneity within cell pop-

Journal of
BIOLOGICAL REGULATORS
and Homeostatic Agents

ulations, and constructing developmental cell trajectories [16,39]. In the present study, we reanalyzed the scRNA-seq dataset proposed by Crnkovic *et al*. [16]. Nature killer (NK) cells, T cells, B cells, dendritic cells (DCs), mast cells, and regulatory T cells (Tregs) were enriched in PAH samples while decreased in normal samples. These findings are consistent with previous study emphasizing the pivotal role of dynamic changes in immune and stromal cells during PAH progression [37]. Furthermore, we observed that POSTN was clustered in fibroblasts and SMCs, and SMC-C07-POSTN was significantly enriched in PAH tissues compared to normal tissues. POSTN emerged as the most differentially expressed gene between PAH and donor SMCs. Additionally, pathways related to ECM-receptor interaction, PI3K-AKT signaling, focal adhesion, and oxidative phosphorylation were notably enriched in SMC-C07-POSTN, indicating the specific enrichment of POSTN$^+$ SMCs in the PAH microenvironment and their association with ECM remodeling.

SMCs constitute a central component of the arterial media and play an essential role in arterial physiology and pathology. Emerging evidence suggests that metabolic and phenotypic switching of SMCs is closely associated with the progression of various vascular diseases, including PH and atherosclerosis [40–42]. The Monocle 2 algorithm was employed to elucidate the dynamic processes of fibroblasts and SMCs at the single-cell level in PAH. We observed the enrichment of PAH cells in the POSTN$^+$ SMC differentiation branch. Moreover, the expressions of genes involved in disease progression-related signaling pathways such as NF-κB, epithelial-mesenchymal transition, apoptosis, and hypoxic pathways were higher in the terminal state of the SMC-C07-POSTN differentiation branch. Notably, in the hypoxic microenvironment, hypoxia-inducible factor 1-alpha (HIF1α) expression and activity were elevated in the regulatory network of POSTN$^+$ SMCs, suggesting its role as a key TF driving this differentiation pathway.

Moreover, we aimed to elucidate the novel mechanism by which POSTN$^+$ SMCs regulate the PAH immune microenvironment. Previous studies have revealed the excessive accumulation of immune cells, including macrophages (Mphs), neutrophils, dendritic cells (DCs), mast cells, T lymphocytes, and B lymphocytes, around the pulmonary vessels of PAH patients [17,21]. Among these, various Mph subtypes play a central role in PAH progression [43]. M1-type Mphs exacerbate inflammation by secreting proinflammatory factors, while M2-type Mphs promote tissue repair. In this study, we observed a strong interaction between SMCs and Mph/Mono in PAH samples. Based on the expression of specific marker genes, seven subtypes were identified within the Mph/Mono lineage. Our findings suggest that POSTN$^+$ SMCs regulate the formation of an inflammatory environment in RGS2$^+$ Mphs via the TGFβ1-SDC2 axis. In summary, a mutually supportive and functionally significant interaction network was established between POSTN$^+$ SMCs and RGS2$^+$ Mphs, potentially contributing to ECM remodeling and promoting an inflammatory environment in PAH. These insights provide novel perspectives into PAH pathogenesis.

However, this study has several limitations. Firstly, the inclusion of public data was limited, and the findings will be validated and reinforced by a larger sample size by establishing an external validation cohort. Secondly, due to constraints in time and funding, the regulatory mechanism of RGS2$^+$ Mphs by POSTN$^+$ SMCs via the TGFβ1-SDC axis, promoting PAH progression, is solely based on bioinformatics analysis. Specific *in vivo* or *in vitro* experimental validation was not conducted. These aspects will be addressed in future investigations.

Conclusions

Our findings provide further evidence on the association between POSTN and PAH through a combination of bioinformatics and experimental methods. We demonstrated, for the first time, the potential involvement of POSTN$^+$ SMCs in regulating the inflammatory microenvironment in RGS2$^+$ Mphs via the TGFβ1-SDC2 axis. These findings also indicate the establishment of a synergistic and functionally significant interaction network between POSTN$^+$ SMCs and RGS2$^+$ Mphs, which may play a pivotal role in ECM remodeling and promotion of the inflammatory environment in PAH. Our findings offer novel insights into PAH pathogenesis.

Abbreviations

PAH, pulmonary arterial hypertension; SMCs, smooth muscle cells; RGS2$^+$, regulator of G protein signaling-2; PH, pulmonary hypertension; ECM, extracellular matrix; PASMCs, pulmonary arterial smooth muscle cells; GEO, Gene Expression Omnibus; scRNA-seq, single-cell RNA sequencing; KEGG, Kyoto Encyclopedia of Genes and Genomes; GSEA, gene set enrichment analysis; TF, transcription factor; Mphs, macrophages; AUC, area under the curve; NK, natural killer; DCs, dendritic cells.

Availability of Data and Materials

The data that support this study are available from the corresponding author on reasonable request.

Author Contributions

LZ, YZ and QG designed the research study; QG performed the research; YZ analyzed the data; QG and YZ drafted the manuscript and all authors have been involved in revising it critically for important intellectual content. All authors gave final approval of the version to be published. All authors have participated sufficiently in the work to take

public responsibility for appropriate portions of the content and agreed to be accountable for all aspects of the work in ensuring that questions related to its accuracy or integrity.

Ethics Approval and Consent to Participate

All institutional and national guidelines for the care and use of laboratory animals were followed and approved by the Committee on the Ethics of Animal Experiments of Nanjing Medical University (approval number: IACUC-2001008).

Acknowledgment

We are grateful to the Department of Forensic Medicine at Nanjing Medical University for providing the samples of Su/Hx PAH models.

Funding

This work was supported by the National Natural Science Foundation of China (NSFC) under Grant [81970723, 81570332], and Key Medical People Project in Jiangsu Province under Grant [ZDRCA2016019].

Conflict of Interest

The authors declare no conflict of interest.

References

[1] Humbert M, Kovacs G, Hoeper MM, Badagliacca R, Berger RMF, Brida M, *et al*. 2022 ESC/ERS Guidelines for the diagnosis and treatment of pulmonary hypertension. European Heart Journal. 2022; 43: 3618–3731.

[2] Ruopp NF, Cockrill BA. Diagnosis and Treatment of Pulmonary Arterial Hypertension: A Review. JAMA. 2022; 327: 1379–1391.

[3] Karia N, Howard L, Johnson M, Kiely DG, Lordan J, McCabe C, *et al*. Predictors of outcomes in mild pulmonary hypertension according to 2022 ESC/ERS Guidelines: the EVIDENCE-PAH UK study. European Heart Journal. 2023; 44: 4678–4691.

[4] Naeije R, Richter MJ, Rubin LJ. The physiological basis of pulmonary arterial hypertension. The European Respiratory Journal. 2022; 59: 2102334.

[5] Imoto K, Okada M, Yamawaki H. Periostin Mediates Right Ventricular Failure through Induction of Inducible Nitric Oxide Synthase Expression in Right Ventricular Fibroblasts from Monocrotaline-Induced Pulmonary Arterial Hypertensive Rats. International Journal of Molecular Sciences. 2018; 20: 62.

[6] Landry NM, Cohen S, Dixon IMC. Periostin in cardiovascular disease and development: a tale of two distinct roles. Basic Research in Cardiology. 2017; 113: 1.

[7] Abdul-Salam VB, Wharton J, Cupitt J, Berryman M, Edwards RJ, Wilkins MR. Proteomic analysis of lung tissues from patients with pulmonary arterial hypertension. Circulation. 2010; 122: 2058–2067.

[8] Kanisicak O, Khalil H, Ivey MJ, Karch J, Maliken BD, Correll RN, *et al*. Genetic lineage tracing defines myofibroblast origin and function in the injured heart. Nature Communications. 2016; 7: 12260.

[9] Cheng N, Wang MY, Wu YB, Cui HM, Wei SX, Liu B, *et al*. Circular RNA POSTN Promotes Myocardial Infarction-Induced Myocardial Injury and Cardiac Remodeling by Regulating miR-96-5p/BNIP3 Axis. Frontiers in Cell and Developmental Biology. 2021; 8: 618574.

[10] Wang XD, Li F, Ma DB, Deng X, Zhang H, Gao J, *et al*. Periostin mediates cigarette smoke extract-induced proliferation and migration in pulmonary arterial smooth muscle cells. Biomedicine & Pharmacotherapy. 2016; 83: 514–520.

[11] Jin S, Guerrero-Juarez CF, Zhang L, Chang I, Ramos R, Kuan CH, *et al*. Inference and analysis of cell-cell communication using CellChat. Nature Communications. 2021; 12: 1088.

[12] Al-Qazazi R, Lima PDA, Prisco SZ, Potus F, Dasgupta A, Chen KH, *et al*. Macrophage-NLRP3 Activation Promotes Right Ventricle Failure in Pulmonary Arterial Hypertension. American Journal of Respiratory and Critical Care Medicine. 2022; 206: 608–624.

[13] Hu L, Wang J, Huang H, Yu Y, Ding J, Yu Y, *et al*. YTHDF1 Regulates Pulmonary Hypertension through Translational Control of MAGED1. American Journal of Respiratory and Critical Care Medicine. 2021; 203: 1158–1172.

[14] Tian L, Wu D, Dasgupta A, Chen KH, Mewburn J, Potus F, *et al*. Epigenetic Metabolic Reprogramming of Right Ventricular Fibroblasts in Pulmonary Arterial Hypertension: A Pyruvate Dehydrogenase Kinase-Dependent Shift in Mitochondrial Metabolism Promotes Right Ventricular Fibrosis. Circulation Research. 2020; 126: 1723–1745.

[15] Sonnenberg-Riethmacher E, Miehe M, Riethmacher D. Periostin in Allergy and Inflammation. Frontiers in Immunology. 2021; 12: 722170.

[16] Crnkovic S, Valzano F, Fließer E, Gindlhuber J, Thekkekara Puthenparampil H, Basil M, *et al*. Single-cell transcriptomics reveals skewed cellular communication and phenotypic shift in pulmonary artery remodeling. JCI Insight. 2022; 7: e153471.

[17] Wang RR, Yuan TY, Wang JM, Chen YC, Zhao JL, Li MT, *et al*. Immunity and inflammation in pulmonary arterial hypertension: From pathophysiology mechanisms to treatment perspective. Pharmacological Research. 2022; 180: 106238.

[18] Southgate L, Machado RD, Gräf S, Morrell NW. Molecular genetic framework underlying pulmonary arterial hypertension. Nature Reviews. Cardiology. 2020; 17: 85–95.

[19] Yang Y, Lin F, Xiao Z, Sun B, Wei Z, Liu B, *et al*. Investigational pharmacotherapy and immunotherapy of pulmonary arterial hypertension: An update. Biomedicine & Pharmacotherapy. 2020; 129: 110355.

[20] Weatherald J, Boucly A, Peters A, Montani D, Prasad K, Psotka MA, *et al*. The evolving landscape of pulmonary arterial hypertension clinical trials. Lancet (London, England). 2022; 400: 1884–1898.

[21] Hu Y, Chi L, Kuebler WM, Goldenberg NM. Perivascular Inflammation in Pulmonary Arterial Hypertension. Cells. 2020; 9: 2338.

[22] Merle B, Garnero P. The multiple facets of periostin in bone metabolism. Osteoporosis International: a Journal Established as Result of Cooperation between the European Foundation for Osteoporosis and the National Osteoporosis Foundation of the USA. 2012; 23: 1199–1212.

[23] Kudo A. The Structure of the Periostin Gene, Its Transcriptional Control and Alternative Splicing, and Protein Expression. Advances in Experimental Medicine and Biology. 2019; 1132: 7–20.

[24] Bonnet N, Garnero P, Ferrari S. Periostin action in bone. Molecular and Cellular Endocrinology. 2016; 432: 75–82.

[25] Zhu R, Zheng Y, Dirks NL, Vadhavkar S, Jin JY, Peng K, *et al*. Model-based clinical pharmacology profiling and exposure-response relationships of the efficacy and biomarker of lebrik-

Journal of
BIOLOGICAL REGULATORS
and Homeostatic Agents

izumab in patients with moderate-to-severe asthma. Pulmonary Pharmacology & Therapeutics. 2017; 46: 88–98.

[26] Asano T, Kanemitsu Y, Takemura M, Yokota M, Fukumitsu K, Takeda N, *et al*. Serum Periostin as a Biomarker for Comorbid Chronic Rhinosinusitis in Patients with Asthma. Annals of the American Thoracic Society. 2017; 14: 667–675.

[27] Hakuno D, Kimura N, Yoshioka M, Mukai M, Kimura T, Okada Y, *et al*. Periostin advances atherosclerotic and rheumatic cardiac valve degeneration by inducing angiogenesis and MMP production in humans and rodents. The Journal of Clinical Investigation. 2010; 120: 2292–2306.

[28] Bülow RD, Boor P. Extracellular Matrix in Kidney Fibrosis: More Than Just a Scaffold. The Journal of Histochemistry and Cytochemistry: Official Journal of the Histochemistry Society. 2019; 67: 643–661.

[29] Bolton K, Segal D, McMillan J, Sanigorski A, Collier G, Walder K. Identification of secreted proteins associated with obesity and type 2 diabetes in Psammomys obesus. International Journal of Obesity (2005). 2009; 33: 1153–1165.

[30] Li X, Sun Z, Peng G, Xiao Y, Guo J, Wu B, *et al*. Single-cell RNA sequencing reveals a pro-invasive cancer-associated fibroblast subgroup associated with poor clinical outcomes in patients with gastric cancer. Theranostics. 2022; 12: 620–638.

[31] Marietta M, Coluccio V, Boriani G, Luppi M. Effects of Anti-vitamin k oral anticoagulants on bone and cardiovascular health. European Journal of Internal Medicine. 2020; 79: 1–11.

[32] Gerbaix M, Ammann P, Ferrari S. Mechanically Driven Counter-Regulation of Cortical Bone Formation in Response to Sclerostin-Neutralizing Antibodies. Journal of Bone and Mineral Research: the Official Journal of the American Society for Bone and Mineral Research. 2021; 36: 385–399.

[33] Wu J, Subbaiah KCV, Xie LH, Jiang F, Khor ES, Mickelsen D, *et al*. Glutamyl-Prolyl-tRNA Synthetase Regulates Proline-Rich Pro-Fibrotic Protein Synthesis During Cardiac Fibrosis. Circulation Research. 2020; 127: 827–846.

[34] Schwanekamp JA, Lorts A, Vagnozzi RJ, Vanhoutte D, Molkentin JD. Deletion of Periostin Protects Against Atherosclerosis in Mice by Altering Inflammation and Extracellular Matrix Remodeling. Arteriosclerosis, Thrombosis, and Vascular Biology. 2016; 36: 60–68.

[35] Wang J, Niu Y, Luo L, Lu Z, Chen Q, Zhang S, *et al*. Decoding ceRNA regulatory network in the pulmonary artery of hypoxia-induced pulmonary hypertension (HPH) rat model. Cell & Bioscience. 2022; 12: 27.

[36] Nie X, Shen C, Tan J, Wu Z, Wang W, Chen Y, *et al*. Periostin: A Potential Therapeutic Target For Pulmonary Hypertension? Circulation Research. 2020; 127: 1138–1152.

[37] Savai R, Pullamsetti SS, Kolbe J, Bieniek E, Voswinckel R, Fink L, *et al*. Immune and inflammatory cell involvement in the pathology of idiopathic pulmonary arterial hypertension. American Journal of Respiratory and Critical Care Medicine. 2012; 186: 897–908.

[38] Tobal R, Potjewijd J, van Empel VPM, Ysermans R, Schurgers LJ, Reutelingsperger CP, *et al*. Vascular Remodeling in Pulmonary Arterial Hypertension: The Potential Involvement of Innate and Adaptive Immunity. Frontiers in Medicine. 2021; 8: 806899.

[39] Hua X, Hu G, Hu Q, Chang Y, Hu Y, Gao L, *et al*. Single-Cell RNA Sequencing to Dissect the Immunological Network of Autoimmune Myocarditis. Circulation. 2020; 142: 384–400.

[40] Li D, Shao NY, Moonen JR, Zhao Z, Shi M, Otsuki S, *et al*. ALDH1A3 Coordinates Metabolism With Gene Regulation in Pulmonary Arterial Hypertension. Circulation. 2021; 143: 2074–2090.

[41] Xu W, Janocha AJ, Erzurum SC. Metabolism in Pulmonary Hypertension. Annual Review of Physiology. 2021; 83: 551–576.

[42] Gorelova A, Berman M, Al Ghouleh I. Endothelial-to-Mesenchymal Transition in Pulmonary Arterial Hypertension. Antioxidants & Redox Signaling. 2021; 34: 891–914.

[43] Zhang MQ, Wang CC, Pang XB, Shi JZ, Li HR, Xie XM, *et al*. Role of macrophages in pulmonary arterial hypertension. Frontiers in Immunology. 2023; 14: 1152881.